



LAWRENCE
LIVERMORE
NATIONAL
LABORATORY

THERMODYNAMICS AND MAGNETISM OF SmFe_{12} COMPOUND DOPED WITH Zr, Ce, Co AND Ni: AN AB INITIO STUDY

A. Landa, P. Soderlind , E. E. Moore, A. Perron

September 30, 2023

Metals

Disclaimer

This document was prepared as an account of work sponsored by an agency of the United States government. Neither the United States government nor Lawrence Livermore National Security, LLC, nor any of their employees makes any warranty, expressed or implied, or assumes any legal liability or responsibility for the accuracy, completeness, or usefulness of any information, apparatus, product, or process disclosed, or represents that its use would not infringe privately owned rights. Reference herein to any specific commercial product, process, or service by trade name, trademark, manufacturer, or otherwise does not necessarily constitute or imply its endorsement, recommendation, or favoring by the United States government or Lawrence Livermore National Security, LLC. The views and opinions of authors expressed herein do not necessarily state or reflect those of the United States government or Lawrence Livermore National Security, LLC, and shall not be used for advertising or product endorsement purposes.

Article

Thermodynamics and Magnetism of SmFe₁₂ Compound Doped with Zr, Ce, Co and Ni: An Ab Initio Study

Alexander Landa *, Per Söderlind, Emily E. Moore and Aurélien Perron

Critical Materials Innovation Hub, Lawrence Livermore National Laboratory, Livermore, CA 94551-0808, USA; soderlind@llnl.gov (P.S.); moore255@llnl.gov (E.E.M.); perron1@llnl.gov (A.P.)

* Correspondence: landa1@llnl.gov

Abstract: Alloys that are Ni-doped, such as the (Sm_{1-y}Zr_y)(Fe_{1-x}Co_x)₁₂ and (Ce_{0.5}Sm_{0.5})Fe₁₀Co₂ systems, are studied because of their magnetic properties. The (Sm_{1-y}Zr_y)(Fe_{1-x}Co_x)_{11-z}Ti_z and (Ce_{0.1-x}Sm_x)Fe₉Co₂Ti alloys are considered contenders for vastly effective permanent magnets because of their anisotropy field and Curie temperature. Ti can act as a stabilizer for the SmFe₁₂ compound but substantially suppresses saturation magnetization. To maintain the saturation magnetization in the scope of 1.3–1.5 T, we propose substituting a particular quantity of Fe and Co in the (Sm_{1-y}Zr_y)(Fe_{1-x}Co_x)₁₂ and (Ce_{0.5}Sm_{0.5})Fe₁₀Co₂ alloys with Ni. By performing ab initio calculations, we show that Ni incorporation results in increased thermodynamic stability and, in contrast to Ti, has a parallel spin moment aligned to the moment of the SmFe₁₂ compound and improves its saturation magnetization without affecting the anisotropy field or Curie temperature.

Keywords: density-functional theory; rare earth elements; permanent magnets; saturated magnetization; anisotropy field; Curie temperature

1. Introduction

Rare earth-based magnets that exhibit the ThMn₁₂-type structure have garnered interest as hard magnetic materials. Specifically, the tetragonal REFe₁₂-based compound, which RE describes as a rare-earth metal, is studied because of its significant saturation magnetization (μ_0M_s), significant anisotropy field (μ_0H_a), and significant Curie temperature (T_c) [1–8]. An REFe₁₂ magnet has a lower RE concentration (7.7 at.%) in contrast to the extensively used Nd₂Fe₁₄B₁ magnet, or so-called Neomax, (11.8 at.%). However, the SmFe₁₂ compound is not considered to be stable from a thermodynamic standpoint in the bulk, but its favorable intrinsic properties, $\mu_0M_s = 1.64$ T, $\mu_0H_a = 12$ T, and $T_c = 550$ K [1], resemble epitaxially grown thin films. To sustain the REFe₁₂ phase in the bulk material, substituting Fe with a stabilizing metal M, where M = Ti, Nb, V, Mo, Cr, Mn, W, Re, Al, Ga, Si, H, and C, has been studied. The composition area x for stabilizing the REFe_{12-x}M_x phase is conditional on M [9].

It is known that Ti is favored to stabilize REFe_{12-x}M_x alloys with x~1 [2]. The samarium-based compound SmFe₁₁Ti₁ has a saturation magnetization $\mu_0M_s = 1.14$ – 1.22 T that is smaller than the saturation magnetization of Nd₂Fe₁₄B₁ ($\mu_0M_s = 1.61$ T) [10,11]. The stabilization of the SmFe₁₂M magnet is supported by considerable contraction of the magnetic moment because the spin addition to the magnetic moment of the stabilizing element aligns itself anti-parallel in direction to the internal magnetization of the SmFe₁₂ intermetallic compound. Therefore, it is critical to keep the concentration of stabilizer as small as possible.

In accordance with the works of Tozman et al. [12], the above-mentioned reduction of the saturated magnetization of the SmFe₁₁Ti₁ compound can be recovered by partial replacement of Fe, e.g., for the Sm(Fe_{0.8}Co_{0.2})₁₁Ti magnet $\mu_0M_s = 1.43$ T [12]. Another practice to enhance the saturation magnetization of the SmFe_{12-x}Ti_x alloys is to reduce the Ti content, where instead the phase stability is assured by Zr or Y partially substituting on

Citation: Landa, A.; Söderlind, P.; Moore, E.E.; Perron, A. Thermodynamics and Magnetism of SmFe₁₂ Compound Doped with Zr, Ce, Co and Ni: An Ab Initio Study. *Metals* **2024**, *14*, x. <https://doi.org/10.3390/xxxxx>

Academic Editor: Giuseppe Laci-dogna

Received: 30 November 2023

Revised: 26 December 2023

Accepted: 29 December 2023

Published: date



Copyright: © 2023 by the authors. Submitted for possible open access publication under the terms and conditions of the Creative Commons Attribution (CC BY) license (<https://creativecommons.org/licenses/by/4.0/>).

the Sm site [13–15]. Kuno et al. [13] presumed that an alloy that includes both Zr and M (for instance, Ti) could stabilize the ThMn₁₂-type magnet with less than a single M atom per formula unit: the strip-cast (Sm_{0.8}Zr_{0.2})(Fe_{0.75}Co_{0.25})_{11.5}Ti_{0.5} magnet reaches a saturation magnetization $\mu_0M_s = 1.58$ T and anisotropy field $\mu_0H_a = 7.41$ T that are identical to those of Neomax ($\mu_0M_s = 1.61$ T, $\mu_0H_a = 7.60$ T) [16], although the Curie temperature of the (Sm_{0.8}Zr_{0.2})(Fe_{0.75}Co_{0.25})_{11.5}Ti_{0.5} magnet, $T_c = 880$ K, substantially surpasses Neomax, $T_c = 584$ K [16]. Further improvement in saturation magnetization is possible for the Sm(Fe_{0.8}Co_{0.2})₁₁Ti compound ($\mu_0M_s = 1.43$ T), which can be accomplished by reducing the Ti content from Ti₁ to Ti_{0.5} and with partial substitution of Sm by Zr as reported by Tozman et al. [12], where the magnetic properties of the (Sm_{0.80}Zr_{0.20})(Fe_{0.80}Co_{0.20})_{11.5}Ti_{0.5} magnet are: $\mu_0M_s = 1.53$ T and $\mu_0H_a = 8.4$ T, with $T_c = 830$ K. Further improvement of Zr substituting for Sm allowed Tozman et al. [17,18] to produce a magnet with a large saturation magnetization, where $\mu_0M_s = 1.90$ T, for the (Sm_{0.82}Zr_{0.18})(Fe_{0.8}Co_{0.2})₁₂ magnet, epitaxially grown thin films with the anisotropy field, $\mu_0H_a = 9.8$ T, and Curie temperature, $T_c = 671$ K.

An excess of cerium metal exists, while its uses do not exceed production, making the mining economics of other less abundant and more technologically important rare earth metals very expensive. Thus, Ce-based magnets with the ThMn₁₂-type intermetallic compound would be perfect candidates for new-rare earth permanent magnets [19–22]. Theoretical analyses have shown that Ce might possibly stabilize the ThMn₁₂-type intermetallic compound [23–27]. Goll et al. [28] found that a CeTiFe_{1-x}Co_x arc melted (and quenched) magnet shows the maximum value of the saturation magnetization, $\mu_0M_s = 1.27$ T, magnetic anisotropy energy (MAE), $K_1 = 2.15$ MJ/m³, and the maximum energy product, $|BH|_{\max} = 282$ kJ/m³, at $x \approx 1.95$, are considerably reduced compared to Neomax ($\mu_0M_s = 1.61$ T, $\mu_0H_a = 7.60$ T, and $|BH|_{\max} \sim 515$ kJ/m³) [16]. In order to increase MAE and thus the coercivity of the CeFe₉Co₂Ti magnets, Gabay et al. [29], Martin-Cid et al. [30], Wuest et al. [31], Martin-Cid et al. [32], and Martin-Cid [33] proposed sectional replacement of Ce with Sm, resulting in the (Ce_{1-x}Sm_x)Ti₁Co₂Fe₉ magnet films synthesized via melt-spinning [27–33]. According to [32,33], for the (Ce_{0.5}Sm_{0.5})Ti₁Co₂Fe₉ magnet: saturation magnetization, $\mu_0M_s = 1.15$ T, anisotropy field, $\mu_0H_a = 5.6$ T, Curie temperature, $T_c = 726$ K, and maximum energy product, $|BH|_{\max} = 261.28$ kJ/m³. Recently, Saito [34] discovered that the compelling increment of the CeFe₁₁Ti melt-spun ribbon coercivity can be reached by partial replacement of Sm with Ce.

In our past works [35–38], we suggest enhancing μ_0M_s and $(BH)_{\max}$ in the widely studied SmCo₅, YCo₅, and SmFe₁₂ magnets by replacing Co with Fe and using Ni as a stabilizer. As mentioned above, the stabilization of the SmFe₁₁M magnet is accompanied by a considerable decrease in the magnetic moment because of the anti-parallel spin alignment of the magnetic moment of a given stabilizing metal, M, to the internal magnetization of the SmFe₁₂ intermetallic compound. On the contrary, the spin moment of Ni exhibits parallel alignment with respect to the internal net magnetization of the SmFe₁₂ compound, thereby increasing its saturation magnetization. Recent calculations [38] demonstrate that the SmNi₄(Fe_{1-x}Co_x)₈ alloys of the ThMn₁₂ type structure could be stable and possibly manufactured in bulk form across the entire compositional range. They have compelling magnetic properties, such as: μ_0M_s values of 1.38–1.57 T, 1.39–1.53 T, and 1.36–1.42 T (model dependent); T_c values of 853 K, 928 K, and 995 K, and μ_0H_a values that are 6.09 T, 8.02 T, and 10.54 T, respectively. However, similar to the case of the undoped SmFe₁₂ magnet, the RE (Sm) content is 7.7 at.% for the SmNi₄(Fe_{1-x}Co_x)₈ alloys. The partial substitution of Sm by Zr or Ce will decrease the content of critical RE.

The primary purpose of the current study is to study the influence of zirconium and cerium on the phase stability of the (Sm,Zr,Ce)(Fe-Co-Ni)₁₂ alloys and to assess their magnetic properties. We perform ab initio calculations using the following formalisms: (i) the fully relativistic exact muffin-tin orbital method (FREMTO) in conjunction with the coherent potential approximation (CPA) and (ii) the full-potential linear muffin-tin orbital method (FP-LMTO), see [35–38] for details. The methods account for all relativistic effects, such as spin-orbit coupling (SOC). These two techniques provide accurate results that are

independent of technical implementation and rely on the particular strength and durability of each technique. The results of the density-functional theory (DFT) calculations of the ground-state properties of the (Sm,Zr,Ce)(Fe-Co-Ni)₁₂ alloys are presented in Section 2. We discuss the results of the DFT calculations and the magnetic characteristics of the (Sm,Zr,Ce)(Fe-Co-Ni)₁₂ alloys in Section 3. Finally, an analysis and summary are presented in Section 4.

2. Thermodynamic Properties of the (Sm,R)Ni₄(Fe,Co)₈ Alloys: R=Zr, Ce

The SmFe₁₂ assumes the body-centered crystal structure is represented by the ThMn₁₂-type structure (space group *I4/mmm*, no. 139; see Figure 1). The structure contains the Sm atom on the 2*a* Wyckoff site, and 12 Fe atoms occupy three inequivalent Wyckoff sites, 8*f*, 8*i*, and 8*j*, respectively. According to the Pearson symbol (*tI26*), the usual SmFe₁₂ supercell contains 26 atoms but can be defined by a reduced supercell with 13 atoms (1 Sm and 12 Fe) used in the present calculations.

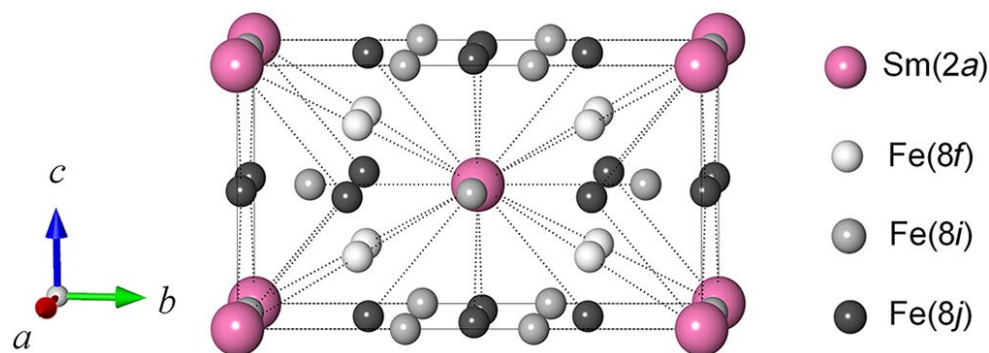


Figure 1. Crystal structure of the SmFe₁₂ (ThMn₁₂-type) compound sketched using Vesta software (version x, manufacturer name, city, country) [39]. The larger pink spheres denote the Sm atoms at Wyckoff position 2*a*, while the smaller white, gray, and black spheres are the Fe atoms at Wyckoff positions 8*f*, 8*i*, and 8*j*, respectively. Adapted with permission from Ref. [40]. Reuse and Permissions License Number: RNP/23/DEC/073479.

As mentioned in Ref. [38], the Sm(Fe_{1-x}Co_x)₁₂ alloys could be stabilized by substituting a particular portion of Fe or Co atoms with Ni atoms. The optimal configuration of these alloys has a stoichiometry of SmNi₄(Fe_{1-x}Co_x)₈, where a single Sm atom occupies the 2*a* Wyckoff position, 4 Ni atoms occupy the 8*j* Wyckoff position, and 8 (Fe_{1-x}Co_x) atoms are randomly distributed on the 8*i* and 8*f* Wyckoff positions (see Figure 1).

To analyze the stabilizing effects of the nickel addition to the (Sm_{0.8}Zr_{0.2})(Fe_{1-x}Co_x)₁₂ compounds, we carried out EMTO-CPA calculations for the formation energy of the (Sm_{0.8}Zr_{0.2})Ni₄(Fe_{1-x}Co_x)₈ compound relative to the reference states for unary systems α -Sm, α -Zr, α -Fe, α -Co, and α -Ni, where Sm and Zr atoms occupy the 2*a* sublattice, 4 Ni atoms occupy the 8*j* sublattice, and occupation of the 8*i* and 8*f* sublattices gradually changes from pure Fe to pure Co metals. As can be seen from Figure 2, the formation energies of the (Sm_{0.8}Zr_{0.2})Ni₄(Fe_{1-x}Co_x)₈ alloys are negative within the whole compositional interval.

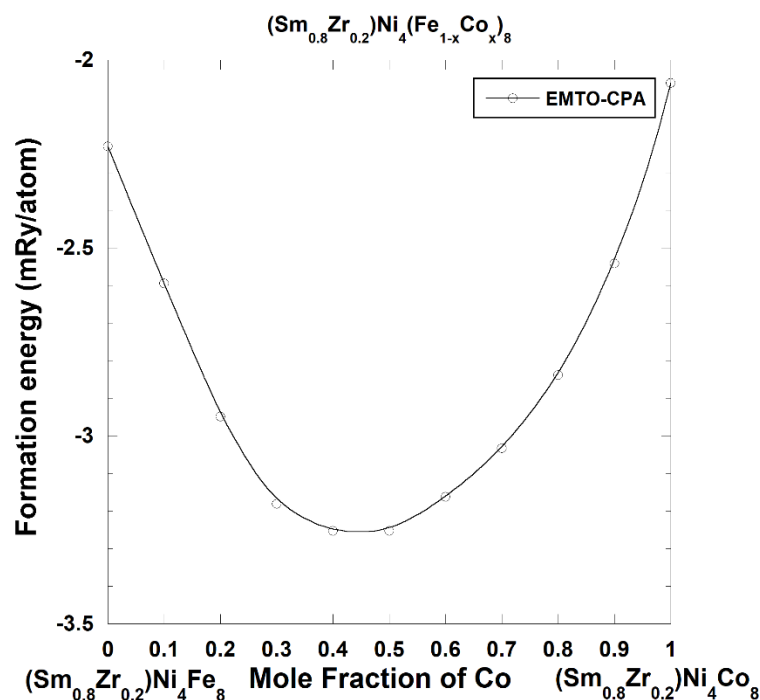


Figure 2. Calculated heat of formation of the quasi-binary $(\text{Sm}_{0.8}\text{Zr}_{0.2})\text{Ni}_4(\text{Fe}_{1-x}\text{Co}_x)_8$ alloys, where Sm and Zr atoms occupy the $2a$ sublattice, 4 Ni atoms occupy the $8j$ sublattice, and 8 (Co,Fe) atoms are randomly distributed on the $8i$ and $8f$ sublattices.

To avoid using the titanium metal as a stabilizer, e.g., $\text{CeFe}_9\text{Co}_2\text{Ti}$ [30–32], we instead used the nickel metal, whose spin moments align parallel to the internal net magnetization of the SmFe_{12} compound, thus enhancing its saturation magnetization. Although Martin-Cid et al. [32] discussed the probabilities of Co atom site occupation for the $(\text{Ce}_{1-x}\text{Sm}_x)\text{Ti}_1\text{Co}_2\text{Fe}_9$ magnets, $x = 0.00, 0.25, 0.50, 0.75,$ and 1.00 , assuming that a single Ti atom occupies an $8i$ Wyckoff position, we estimated the lowest energy configuration for the $\text{CeNi}_4\text{Co}_2\text{Fe}_6$ magnet assuming that 4 Ni atoms occupy $8j$ Wyckoff positions in analogy with the calculated energetically favorable configuration for the $\text{SmNi}_4(\text{Fe}_{1-x}\text{Co}_x)_8$ alloys [38]. The EMTO-CPA calculations for the $\text{CeNi}_4\text{Co}_2\text{Fe}_6$ magnet revealed (see Table 1) that the configuration, where 2 Fe and 2 Co atoms occupy the $8f$ Wyckoff positions, 4 Fe atoms occupy the $8i$ Wyckoff positions, and 4 Ni atoms occupy the $8j$ Wyckoff positions, is the energetically favorable configuration.

Table 1. The relative energies of different $\text{CeNi}_4\text{Co}_2\text{Fe}_6$ magnet atomic configurations. The energy of the $\text{CeNi}_4\text{Co}_2\text{Fe}_6$ magnet, where 2 Fe and 2 Co atoms occupy the $8f$ Wyckoff positions, 4 Fe atoms occupy the $8i$ Wyckoff positions, and 4 Ni atoms occupy the $8j$ Wyckoff positions, is taken to be zero.

Configuration	ΔE (mRy/Atom)
$\text{Ce}(\text{Fe}_2\text{Co}_2)_{8f}(\text{Fe}_4)_{8i}(\text{Ni}_4)_{8j}$	0.000
$\text{Ce}(\text{Fe}_{0.75}\text{Co}_{0.25})_{8f8j}(\text{Ni}_4)_{8j}$	0.470
$\text{Ce}(\text{Fe}_3\text{Co}_1)_{8f}(\text{Fe}_3\text{Co}_1)_{8i}(\text{Ni}_4)_{8j}$	0.642
$\text{Ce}(\text{Fe}_4)_{8f}(\text{Fe}_2\text{Co}_2)_{8i}(\text{Ni}_4)_{8j}$	1.068

To investigate the stabilizing effects of nickel additions to the $(\text{Ce}_{1-x}\text{Sm}_x)\text{Fe}_{10}\text{Co}_2$ alloys, we carried out EMTO-CPA calculations of the formation energy of the $(\text{Ce}_{1-x}\text{Sm}_x)\text{Ni}_4\text{Fe}_6\text{Co}_2$ alloys in respect to the reference states for unary systems α -Sm, α -Ce, α -Fe, α -Co, and α -Ni, where Ce and Sm atoms are randomly distributed on the $2a$ Wyckoff positions, 2 Fe and 2 Co atoms occupy the $8f$ Wyckoff positions, 4 Fe atoms occupy the $8i$

Wyckoff positions, and 4 Ni atoms occupy the 8j Wyckoff positions, within the whole compositional interval ($0 \leq x \leq 1$). The results of these calculations are shown in Figure 3. The calculations show the negative heat of formation of the $(\text{Ce}_{1-x}\text{Sm}_x)\text{Ni}_4\text{Fe}_6\text{Co}_2$ alloys across the whole compositional interval, suggesting the possibility of the creation of bulk magnets. Notice that the experiments [28–34] resulted in the synthesizing of the melt-spun ribbons.

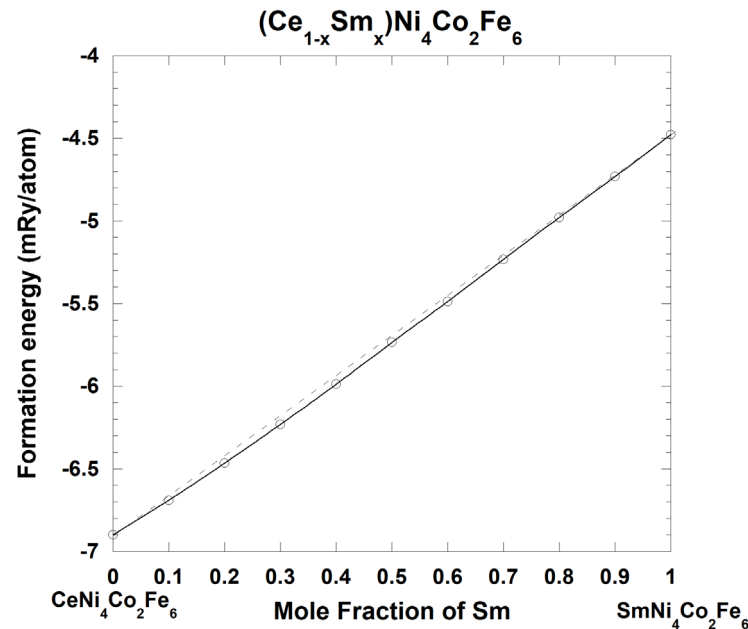


Figure 3. Calculated heat of formation of the quasi-binary $(\text{Ce}_{1-x}\text{Sm}_x)\text{Ni}_4\text{Co}_2\text{Fe}_6$ alloys where Ce and Sm atoms are randomly distributed on the 2a Wyckoff positions, 2 Fe and 2 Co atoms occupy the 8f Wyckoff positions, 4 Fe atoms occupy the 8i Wyckoff positions, and 4 Ni atoms occupy the 8j Wyckoff positions.

3. Magnetic Properties of the $(\text{Sm},\text{R})\text{Ni}_4(\text{Fe},\text{Co})_8$ Alloys: $\text{R}=\text{Zr}, \text{Ce}$

The total moment of the $(\text{Sm}_{0.8}\text{Zr}_{0.2})\text{Ni}_4\text{Fe}_8$ compound, where Sm and Zr atoms occupy the 2a sublattice, 4 Ni atoms occupy the 8j sublattice, and 8 Fe atoms are equally distributed on the 8i and 8f sublattices, calculated in this study using the FREMTO-CPA method, is equal to ($m^{\text{total}} \approx 21.5431 \mu_B/f.u.$) at the equilibrium volume ($\Omega_0 = 13.499 \text{ \AA}^3$). Taking into consideration the calculated total moment per atom ($m_{\text{at.}}^{\text{tot}} = 1.6572 \mu_B$) and the calculated density of the $(\text{Sm}_{0.8}\text{Zr}_{0.2})\text{Ni}_4\text{Fe}_8$ compound ($\rho = 7.760 \text{ g/cm}^3$), one can evaluate $M_s = m_{\text{at.}}^{\text{tot}} [\mu_B] \frac{\rho N_A}{M_{(\text{Sm}_{0.8}\text{Zr}_{0.2})\text{Ni}_4\text{Fe}_8}} = 1.1385 \text{ MA/m}$ and $\mu_0 M_s = 1.4307 \text{ T}$, where $\mu_B = 9.274 \times 10^{-24} \text{ Am}^2$, $[\mu_B]$ is the dimension for μ_B , $N_A = 6.0221 \times 10^{23} \text{ atoms/mole}$, and $M_{(\text{Sm}_{0.8}\text{Zr}_{0.2})\text{Ni}_4\text{Fe}_8} = 63.0819 \text{ g/mol}$ (the average atomic weight per atom of the $(\text{Sm}_{0.8}\text{Zr}_{0.2})\text{Ni}_4\text{Fe}_8$ compound). Thus, the maximum energy product of the $(\text{Sm}_{0.8}\text{Zr}_{0.2})\text{Ni}_4\text{Fe}_8$ compound is $|BH|_{\text{max}} = \frac{1}{4} \mu_0 M_s^2 = 407.207 \text{ kJ/m}^3$, where $\mu_0 = 4\pi \times 10^{-7} \frac{\text{kg}\cdot\text{m}}{\text{sec}^2\text{A}^2}$ is the permeability of free space.

By sequentially replacing Fe with Co from $(\text{Sm}_{0.8}\text{Zr}_{0.2})\text{Ni}_4\text{Fe}_8$ to $(\text{Sm}_{0.8}\text{Zr}_{0.2})\text{Ni}_4\text{Co}_8$, the calculated (FREMTO-CPA) site-projected spin ($m^{(s)}$) and orbital moments ($m^{(o)}$), as well as the total moments ($m^{\text{tot.}}$) of the $(\text{Sm}_{0.8}\text{Zr}_{0.2})\text{Ni}_4(\text{Fe}_{0.9}\text{Co}_{0.1})_8$, $(\text{Sm}_{0.8}\text{Zr}_{0.2})\text{Ni}_4(\text{Fe}_{0.8}\text{Co}_{0.2})_8$, and $(\text{Sm}_{0.8}\text{Zr}_{0.2})\text{Ni}_4\text{Co}_8$ compounds, where 4 Ni atoms occupy the 8j sublattice and 8 $(\text{Fe}_{1-x}\text{Co}_x)$ atoms are equitably distributed on the 8i and 8f sublattices, are presented in Table 2.

Table 2. Site-projected spin ($m^{(s)}$) and orbital ($m^{(o)}$) magnetic moments for the $(\text{Sm}_{0.8}\text{Zr}_{0.2})\text{Ni}_4\text{Fe}_8$, $(\text{Sm}_{0.8}\text{Zr}_{0.2})\text{Ni}_4(\text{Fe}_{0.9}\text{Co}_{0.1})_8$, $(\text{Sm}_{0.8}\text{Zr}_{0.2})\text{Ni}_4(\text{Fe}_{0.8}\text{Co}_{0.2})_8$, and $(\text{Sm}_{0.8}\text{Zr}_{0.2})\text{Ni}_4\text{Co}_8$ compounds, where Sm and Zr atoms occupy the 2a sublattice, 4 Ni atoms occupy the 8j sublattice, and 8 (Co,Fe) atoms are randomly distributed on the 8i and 8f sublattices. $m^{\text{tot.}} = 21.5431, 21.5747, 20.5341, \text{ and } 14.0884 \mu_B/\text{f.u.}$, respectively.

Header	$\text{Sm}_1(2a)/\text{Zr}_1(2a)$	$\text{Fe}_1(8f)/\text{Co}_1(8f)$	$\text{Fe}_2(8i)/\text{Co}_2(8i)$	$\text{Ni}_3(8j)$
$(\text{Sm}_{0.8}\text{Zr}_{0.2})\text{Ni}_4\text{Fe}_8$				
$m^{(s)} (\mu_B)$	+3.6760/+0.4193	-2.3803/-	-2.3076/-	-0.6086
$m^{(o)} (\mu_B)$	-3.2160/+0.0522	-0.0670/-	-0.0789/-	-0.0591
$(\text{Sm}_{0.8}\text{Zr}_{0.2})\text{Ni}_4(\text{Fe}_{0.9}\text{Co}_{0.1})_8$				
$m^{(s)} (\mu_B)$	+3.6430/+0.4290	-2.4416/-1.5617	-2.3364/-1.4195	-0.6089
$m^{(o)} (\mu_B)$	-3.2713/+0.0411	-0.06558/-0.0986	-0.0740/-0.0876	-0.0572
$(\text{Sm}_{0.8}\text{Zr}_{0.2})\text{Ni}_4(\text{Fe}_{0.8}\text{Co}_{0.2})_8$				
$m^{(s)} (\mu_B)$	+3.7200/+0.4205	-2.24451/-1.5511	-2.3554/-1.4329	-0.6047
$m^{(o)} (\mu_B)$	-3.2913/+0.0364	-0.0657/-0.0970	-0.0714/-0.0870	-0.0537
$(\text{Sm}_{0.8}\text{Zr}_{0.2})\text{Ni}_4\text{Co}_8$				
$m^{(s)} (\mu_B)$	+4.2200/+0.3425	-/-1.5670	-/-1.5001	-0.5530
$m^{(o)} (\mu_B)$	-2.8153/+0.0186	-/-0.0910	-/-0.0734	-0.0366

The FPLMTO (SRM + OP) calculated magnetic properties of the $(\text{Sm}_{0.75}\text{Zr}_{0.25})\text{Ni}_4(\text{Fe}_{1-x}\text{Co}_x)_8$ alloys are also presented in Table 3. Abbreviation SRM + OP stays for the standard rare-earth model + orbital polarization (see Ref. [38] for details).

Table 3. Atomic volume (Ω_0), density (ρ), total moment ($m^{\text{tot.}}$), saturation magnetization (M_s and $\mu_0 M_s$), and maximum energy product ($|BH|_{\text{max}}$) of the $(\text{Sm}_{1-y}\text{Zr}_y)\text{Ni}_4(\text{Fe}_{1-x}\text{Co}_x)_8$ magnets as calculated by the FREMTO-CPA method and using the FPLMTO (SRM + OP) method.

Material	Theory	Ω_0 (\AA^3)	ρ ($\frac{\text{g}}{\text{cm}^3}$)	$m^{\text{tot.}}$ ($\frac{\mu_B}{\text{f.u.}}$)	M_s ($\frac{\text{MA}}{\text{m}}$)	$\mu_0 M_s$ (T)	$ BH _{\text{max}}$ ($\frac{\text{kJ}}{\text{m}^3}$)
$(\text{Sm}_{0.8}\text{Zr}_{0.2})\text{Ni}_4\text{Fe}_8$	FREMTO-CPA	13.50	7.760	21.543	1.139	1.431	407.207
$(\text{Sm}_{0.75}\text{Zr}_{0.25})\text{Ni}_4\text{Fe}_8$	SRM + OP	12.81	8.148	21.190	1.180	1.483	437.435
$(\text{Sm}_{0.8}\text{Zr}_{0.2})\text{Ni}_4(\text{Fe}_{0.9}\text{Co}_{0.1})_8$	FREMTO-CPA	13.49	7.783	21.575	1.140	1.433	408.401
$(\text{Sm}_{0.75}\text{Zr}_{0.25})\text{Ni}_4(\text{Fe}_{0.9}\text{Co}_{0.1})_8$	SRM + OP	12.81	8.196	20.800	1.157	1.454	420.549
$(\text{Sm}_{0.8}\text{Zr}_{0.2})\text{Ni}_4(\text{Fe}_{0.8}\text{Co}_{0.2})_8$	FREMTO-CPA	13.36	7.888	20.534	1.097	1.378	377.691
$(\text{Sm}_{0.75}\text{Zr}_{0.25})\text{Ni}_4(\text{Fe}_{0.8}\text{Co}_{0.2})_8$	SRM + OP	12.81	8.227	20.410	1.137	1.429	406.135
$(\text{Sm}_{0.8}\text{Zr}_{0.2})\text{Ni}_4\text{Co}_8$	FREMTO-CPA	12.59	8.573	14.088	0.799	1.003	200.268
$(\text{Sm}_{0.75}\text{Zr}_{0.25})\text{Ni}_4\text{Co}_8$	SRM + OP	12.75	8.463	15.210	0.851	1.069	227.515

The compositional dependence of $\mu_0 M_s$ and $|BH|_{\text{max}}$ of the $(\text{Sm}_{0.8}\text{Zr}_{0.2})\text{Ni}_4(\text{Fe}_{1-x}\text{Co}_x)_8$ alloys for $x = 0.0, 0.1, 0.2, \text{ and } 1.0$ is presented in Figures 4 and 5, respectively. $\mu_0 M_s$ first increases and approaches the maximum at $x = 0.1$. A further Co concentration increase prompts an acute decrease in $\mu_0 M_s$. The calculated tendency for $|BH|_{\text{max}}$ as a function of the Co replacement is analogous to $\mu_0 M_s$.

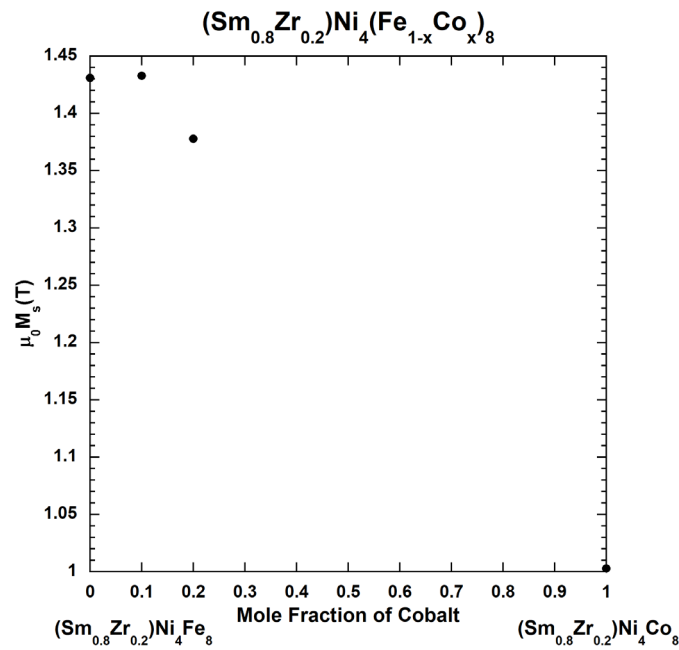


Figure 4. The saturation magnetization of the $(\text{Sm}_{0.8}\text{Zr}_{0.2})\text{Ni}_4(\text{Fe}_{1-x}\text{Co}_x)_8$ alloys, $x = 0.0, 0.1, 0.2, 1.0$.

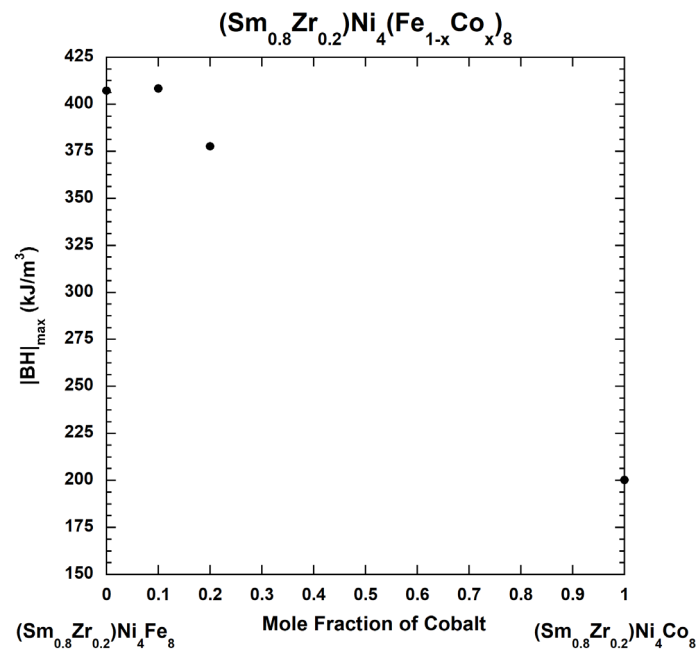


Figure 5. The maximum energy product of the $(\text{Sm}_{0.8}\text{Zr}_{0.2})\text{Ni}_4(\text{Fe}_{1-x}\text{Co}_x)_8$ alloys, $x = 0.0, 0.1, 0.2, 1.0$.

With regards to the Curie temperature (T_c), a mean-field approximation (MFA) can be expressed as [41,42]:

$$T_c = \frac{2}{3} \times \frac{E_{tot}^{DLM} - E_{tot}^{FiM}}{k_B} \quad (1)$$

where E_{tot}^{DLM} and E_{tot}^{FiM} are the ground-state total energies of the DLM (disordered local moment, see Ref. [38] for details) and FiM (ferrimagnetic) states, respectively, and k_B is the Boltzmann constant. Therefore, an evaluation of T_c can be based on the total energy difference between the ferrimagnetic and paramagnetic (DLM) states. Nonetheless, in line with [42], the diversity between the total energies can be substituted by the diversity between the effective single-particle (one atomic specie) energies, which are directly

associated with DLM and FiM states (the so-called MFA treatment). In this paper, E_{tot}^{DLM} and E_{tot}^{FiM} are calculated at the equilibrium volumes for DLM and FiM states, correspondingly.

Figure 6 shows the calculated (within the FREMTO-CPA formalism) T_c values of the pseudo-binary $(\text{Sm}_{0.8}\text{Zr}_{0.2})\text{Ni}_4(\text{Fe}_{1-x}\text{Co}_x)_8$ alloys, where 4 Ni atoms occupy the $8j$ sublattice and 8 $(\text{Fe}_{1-x}\text{Co}_x)$ atoms are distributed on the $8i$ and $8f$ sublattices. The calculated T_c values are equal to 730 K, 792 K, 828 K, and 955 K for the $(\text{Sm}_{0.8}\text{Zr}_{0.2})\text{Ni}_4\text{Fe}_8$, $(\text{Sm}_{0.8}\text{Zr}_{0.2})\text{Ni}_4(\text{Fe}_{0.9}\text{Co}_{0.1})_8$, $(\text{Sm}_{0.8}\text{Zr}_{0.2})\text{Ni}_4(\text{Fe}_{0.8}\text{Co}_{0.2})_8$, and $(\text{Sm}_{0.8}\text{Zr}_{0.2})\text{Ni}_4\text{Co}_8$ alloys, respectively. These values are significantly higher than the Curie temperature of the Neomax ($\text{Nd}_2\text{Fe}_{14}\text{B}_1$) magnet (588 K) [16].

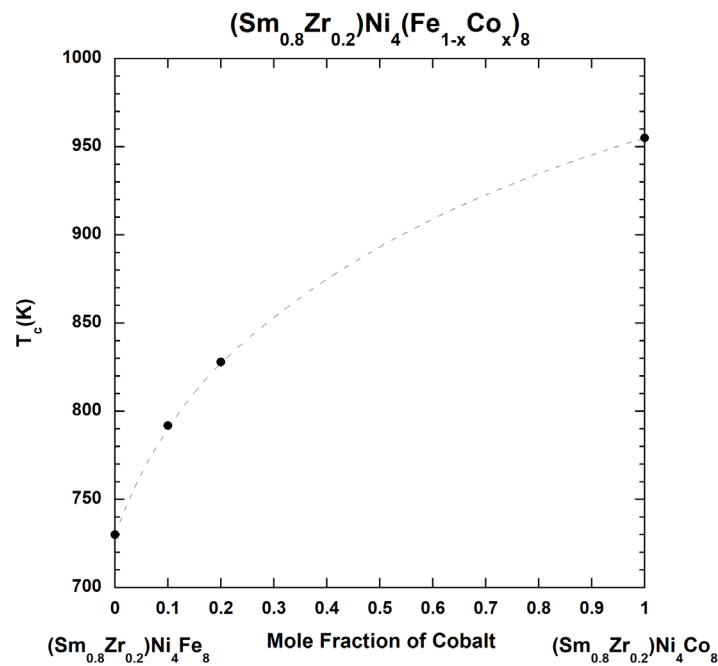


Figure 6. The Curie temperature of the $(\text{Sm}_{0.8}\text{Zr}_{0.2})\text{Ni}_4(\text{Fe}_{1-x}\text{Co}_x)_8$ alloys, $x = 0.0, 0.1, 0.2, 1.0$.

Calculated Curie temperature of the suggested $(\text{Sm}_{0.8}\text{Zr}_{0.2})\text{Ni}_4(\text{Fe}_{0.8}\text{Co}_{0.2})_8$ magnet, $T_c = 828$ K, which is of the same magnitude as the Curie temperature of the zirconium-doped $(\text{Sm}_{0.77}\text{Zr}_{0.24})(\text{Fe}_{0.80}\text{Co}_{0.19})_{11.5}\text{Ti}_{0.65}$ magnet, $T_c = 830$ K Tozman et al. [12], $(\text{Sm}_{0.92}\text{Zr}_{0.08})(\text{Fe}_{0.75}\text{Co}_{0.25})_{11.35}\text{Ti}_{0.65}$ magnet, $T_c = 843$ K Gabay et al. [3], and $(\text{Sm}_{0.8}\text{Zr}_{0.2})(\text{Fe}_{0.75}\text{Co}_{0.25})_{11.5}\text{Ti}_{0.5}$ magnet, $T_c = 880$ K Kuno et al. [13], or yttrium-doped $(\text{Sm}_{0.8}\text{Y}_{0.2})(\text{Fe}_{0.8}\text{Co}_{0.2})_{11.5}\text{Ti}_{0.5}$ magnet, $T_c = 820$ K Hagiwara et al. [14]. All these synthesized magnets contain titanium, which decreases saturation magnetization. The suggested $(\text{Sm}_{0.8}\text{Zr}_{0.2})\text{Ni}_4(\text{Fe}_{0.8}\text{Co}_{0.2})_8$ magnets do not have this deficiency due to a lack of titanium and a credible alignment of nickel magnetic moments.

The calculated (FREMTO-CPA) site-projected spin ($m^{(s)}$) and orbital moments ($m^{(o)}$), as well as the total moments ($m^{(total)}$) of the $(\text{Ce}_{0.5}\text{Sm}_{0.5})\text{Ni}_4\text{Fe}_6\text{Co}_2$ magnet where Ce and Sm atoms equally occupy $2a$ Wyckoff positions, 2 Fe and 2 Co atoms occupy the $8f$ Wyckoff positions, 4 Fe atoms occupy the $8i$ Wyckoff positions, and 4 Ni atoms occupy the $8j$ Wyckoff positions, are presented in Table 4.

Table 4. Site-projected spin ($m^{(s)}$) and orbital ($m^{(o)}$) magnetic moments for the $(\text{Ce}_{0.5}\text{Sm}_{0.5})\text{Ni}_4\text{Fe}_6\text{Co}_2$ magnet, where Ce and Sm atoms equally occupy $2a$ Wyckoff positions, 2 Fe and 2 Co atoms occupy the $8f$ Wyckoff positions, 4 Fe atoms occupy the $8i$ Wyckoff positions, and 4 Ni atoms occupy the $8j$ Wyckoff positions. $M^{\text{tot}} = 20.8942 \mu_B/\text{f.u.}$

$(\text{Ce}_{0.5}\text{Sm}_{0.5})\text{Ni}_4\text{Fe}_6\text{Co}_2$	$\text{Ce}_1(2a)$	$\text{Sm}_1(2a)$	$\text{Fe}_1(8f)$	$\text{Co}_1(8f)$	$\text{Fe}_2(8i)$	$\text{Ni}_3(8j)$
$m^{(s)} (\mu_B)$	+0.1564	+2.2586	-2.3247	-1.5709	-2.3645	-0.6108
$m^{(o)} (\mu_B)$	+0.0159	-3.1577	-0.0658	-0.0930	-0.0699	-0.0608

According to our FREMTO-CPA calculations, the total magnetic moment of the $(\text{Ce}_{0.5}\text{Sm}_{0.5})\text{Ni}_4\text{Fe}_6\text{Co}_2$ compound is equal to $m^{\text{total}} \approx 20.8910 \mu_B/\text{f.u.}$ at an equilibrium atomic volume $\Omega_0 \approx 13.4473 \text{ \AA}^3$. Taking into consideration the calculated total moment per atom, $m_{\text{at.}}^{\text{tot}} = 1.6073 \mu_B$, and the calculated density of the $(\text{Ce}_{0.5}\text{Sm}_{0.5})\text{Ni}_4\text{Fe}_6\text{Co}_2$ compound, $\rho \approx 7.9120 \text{ g/cm}^3$, one can evaluate $M_s \approx 1.1085 \text{ MA/m}$, $\mu_0 M_s = 1.3929 \text{ T}$, and $|BH|_{\text{max}} = 385.992 \text{ kJ/m}^3$. The FREMTO-CPA and FPLMTO (SRM + OP) calculated magnetic properties of the $(\text{Ce}_{0.5}\text{Sm}_{0.5})\text{Ni}_4\text{Fe}_6\text{Co}_2$ compound are shown in Table 5.

Table 5. Atomic volume (Ω_0), density (ρ), total moment (m^{total}), saturation magnetization (M_s and $\mu_0 M_s$), and maximum energy product ($|BH|_{\text{max}}$) of the $(\text{Ce}_{0.5}\text{Sm}_{0.5})\text{Ni}_4\text{Fe}_6\text{Co}_2$ magnet as calculated by the FREMTO-CPA method and using the FPLMTO method and SRM + OP.

Material	Theory	$\Omega_0 (\text{ \AA}^3)$	$\rho (\frac{\text{g}}{\text{cm}^3})$	$m^{\text{total}} (\frac{\mu_B}{\text{f.u.}})$	$M_s (\frac{\text{MA}}{\text{m}})$	$\mu_0 M_s (\text{T})$	$ BH _{\text{max}} (\frac{\text{kJ}}{\text{m}^3})$
$(\text{Ce}_{0.5}\text{Sm}_{0.5})\text{Ni}_4\text{Fe}_6\text{Co}_2$	FREMTO-CPA	13.45	7.912	20.894	1.109	1.393	385.992
	SRM + OP	13.71	7.756	20.020	1.042	1.311	341.757

The mentioned saturation magnetization, $M_s = m_{\text{at.}}^{\text{tot.}} [\mu_B] \frac{\rho N_A}{M} = m_{\text{at.}}^{\text{tot.}} [\mu_B] \frac{N_A}{V} = \frac{m_{\text{at.}}^{\text{tot.}}}{\Omega_0} [\mu_B]$, where $V = \Omega_0 N_A$ is the molar volume, represents the saturation magnetization calculated per atomic volume Ω_0 . The expression $M_s = m_{\text{at.}}^{\text{tot.}} [\mu_B] \frac{N_A}{M}$ represents the saturation magnetization per unit mass. According to the present FREMTO-CPA calculations, the saturation magnetization per unit mass for the $(\text{Ce}_{0.5}\text{Sm}_{0.5})\text{Ni}_4\text{Fe}_6\text{Co}_2$ magnet, $M_s \approx 140.096 \frac{\text{Am}^2}{\text{kg}}$. According to Refs. [32,33], the saturation magnetization of the $(\text{Ce}_{0.5}\text{Sm}_{0.5})\text{Ti}_1\text{Fe}_9\text{Co}_2$ magnet is equal to $M_s = 117 \frac{\text{Am}^2}{\text{kg}}$. Thus, the saturation magnetization and maximum energy product of the suggested $(\text{Ce}_{0.5}\text{Sm}_{0.5})\text{Ni}_4\text{Fe}_6\text{Co}_2$ magnet are 1.197 and 1.434 times larger than the saturation magnetization and maximum energy product of the $(\text{Ce}_{0.5}\text{Sm}_{0.5})\text{Ti}_1\text{Fe}_9\text{Co}_2$ magnet, respectively [30,32,33].

Calculated in a mean-field approximation (FREMTO-CPA), the Curie temperature of the $(\text{Ce}_{0.5}\text{Sm}_{0.5})\text{Ni}_4\text{Fe}_6\text{Co}_2$ magnet is $T_c = 731.89 \text{ K}$.

One crucial quantity for an efficient and realistic magnet is how robust the direction of its magnetic field is. This property is measured or calculated in terms of magnetic anisotropy energy, i.e., the energy difference between the easy (higher energy) and hard (lower energy) directions. Naturally, these energies are very small relative to the total electronic energy of the compound, and to resolve the difference, the energies must be converged to at least 12 digits.

Here, we apply the SRM + OP model for the MAE because the other approximations ($4f$ -band) produce an unreal large MAE due to the improper handling of the $4f$ electrons. Because the MAE is sensitive to the details of the crystal structure, we optimize the parameters, including the atomic volume, to produce the lowest total energy (structural relaxation). Namely, both the lattice parameters a and c are optimized to give the lowest total energy of the tetragonal crystal. These parameters are presented in Table 6. The differences between a and c for the iron-rich compound $(\text{Sm}_{0.75}\text{Zr}_{0.25})\text{Ni}_4(\text{Fe}_{1-x}\text{Co}_x)_8$ (here $x = 0, 0.1, \text{ and } 0.2$) are indeed very small, while for $x = 1$, the total atomic volume diminishes by about 4%.

Table 6. Calculated crystal-structure parameters. Lattice constant a is in units of Å. x_1 and x_2 are atomic position parameters for the 3d-metal components.

Compound	a	c/a	x_1	x_2
(Sm _{0.75} Zr _{0.25} Ni ₄ Fe ₈)	8.4249	0.557	0.359	0.277
(Sm _{0.75} Zr _{0.25})Ni ₄ (Fe _{0.9} Co _{0.1}) ₈	8.4249	0.557	0.359	0.277
(Sm _{0.75} Zr _{0.25})Ni ₄ (Fe _{0.8} Co _{0.2}) ₈	8.4249	0.557	0.359	0.277
(Sm _{0.75} Zr _{0.25})Ni ₄ Co ₈	8.3107	0.560	0.358	0.277
(Ce _{0.5} Sm _{0.5})Ni ₄ Fe ₆ Co ₂	8.6443	0.552	0.361	0.277

There have been numerous attempts to calculate MAE accurately in rare-earth *TM* (*TM*-transition metal) systems. We found an efficient yet accurate procedure to do this in our previous investigation of the SmCo₅-type permanent magnets [35]. Specifically, treat the correlated 4f electrons on the rare-earth atom within the standard rare-earth model while including orbital polarization on the d electrons for the other atoms to ensure better orbital magnetic moments. The entire procedure is free of any parameters.

Calculating (FPLMTO) the total energy for the [001] and [100] spin directions of the 52-atom cell, we obtain the MAE that is listed in Table 7. We also present the calculated anisotropy field, $\mu_0 H_a = 2 K_1/M_s$, [43] and magnetic hardness parameter of the materials, $\kappa = \sqrt{\left(\frac{K_1}{\mu_0 M_s^2}\right)} = \sqrt{\frac{\mu_0 H_a}{2\mu_0 M_s}}$, [43]. As is expected, the MAE increases with increasing Co content, and the reason is simply that Co has a larger orbital moment than Fe.

Table 7. Calculated (FPLMTO: assuming the SRM+OP model) atomic volume, magnetic anisotropy energy, first anisotropy constant, anisotropy field, and magnetic hardness parameter for the (Sm_{0.75}Zr_{0.25})Ni₄(Fe_{1-x}Co_x)₈ alloys, where $x = 0, 0.1, 0.2$, and 1, and (Ce_{0.5}Sm_{0.5})Ni₄Fe₆Co₂ compound.

Compound	Ω_0 (Å ³)	MAE $\left(\frac{\text{meV}}{\text{f. u.}}\right)$	K_1 $\left(\frac{\text{MJ}}{\text{m}^3}\right)$	$\mu_0 H_a$ (T)	κ
(Sm _{0.75} Zr _{0.25} Ni ₄ Fe ₈)	12.81	0.592	0.570	0.966	0.571
(Sm _{0.75} Zr _{0.25})Ni ₄ (Fe _{0.9} Co _{0.1}) ₈	12.81	1.520	1.464	2.531	0.933
(Sm _{0.75} Zr _{0.25})Ni ₄ (Fe _{0.8} Co _{0.2}) ₈	12.81	2.529	2.435	4.283	1.214
(Sm _{0.75} Zr _{0.25})Ni ₄ Co ₈	12.75	2.816	2.724	6.402	1.730
(Sm _{0.5} Ce _{0.5})Ni ₄ Fe ₆ Co ₂	13.71	6.695	6.027	11.568	2.101

According to [43,44], the interchange between magnetic anisotropy and saturation magnetization defines resistance to the self-demagnetization of a magnet fabricated in any possible shape. The empirical rule requires $\kappa \geq 1$ for good permanent magnet fabrication. As can be seen from Table 7, the (Sm_{0.75}Zr_{0.25})Ni₄(Fe_{0.8}Co_{0.2})₈, (Sm_{0.75}Zr_{0.25})Ni₄Co₈, and (Sm_{0.5}Ce_{0.5})Ni₄Fe₆Co₂ magnets meet the manufacturability standards (i.e., $\kappa \geq 1$).

In Table 8, we compare the results of our calculations for the (Sm_{0.5}Ce_{0.5})Ni₄Fe₆Co₂ magnet with the experimental data for the melt-spun magnetic ribbons (Ce_{0.5}Sm_{0.5})Fe₉Co₂Ti, [32,33]. Both magnets have almost identical Curie temperatures; however, the suggested (Ce_{0.5}Sm_{0.5})Ni₄Fe₆Co₂ magnet has a much higher anisotropy field and a higher maximum energy product. In both cases, $k > 1$, which satisfies an empirically required rule to manufacture a strong permanent magnet.

Table 8. Calculated (FPLMTO) saturated magnetization, anisotropy field, Curie temperature, maximum energy product, and magnetic hardness parameter for the (Ce_{0.5}Sm_{0.5})Ni₄Fe₆Co₂ compound compared to the experimental data for the (Ce_{0.5}Sm_{0.5})Fe₉Co₂Ti melt-spun magnetic ribbon [32,33].

Material	$\mu_0 M_s$ (T)	$\mu_0 H_a$ (T)	T_c (K)	$ BH _{max}$ (kJ/m ³)	κ
(Sm _{0.5} Ce _{0.5})Ni ₄ Fe ₆ Co ₂	1.311	11.57	731.89	341.575	2.101
(Ce _{0.5} Sm _{0.5})Fe ₉ Co ₂ Ti	1.150	5.60	726.00	261.380	1.560

4. Discussion and Conclusions

The material of interest should satisfy the following magnetic property conditions to be considered a viable hard permanent magnet: $\mu_0 M_s \sim \geq 1.25$ T, $T_c \sim \geq 550$ K, $\mu_0 H_a \sim \geq 3.75$ T, and $\kappa > 1$ [1,43]. The present calculations show that the $(\text{Sm}_{0.8}\text{Zr}_{0.2})\text{Ni}_4(\text{Fe}_{1-x}\text{Co}_x)_8$ alloys are stable across the entire compositional range and have large $\mu_0 M_s$ values between 1.43–1.48 T (depending on the model); T_c values of 730 K, 792 K, 828 K, and 955 K; $\mu_0 H_a$ values of 0.966 T, 2.531 T, 4.283 T, and 6.421 T; and κ values of 0.571, 0.933, 1.214, 1.730, for $x = 0.0, 0.1, 0.2,$ and $1.0,$ respectively. For the $(\text{Ce}_{0.5}\text{Sm}_{0.5})\text{Ni}_4\text{Fe}_6\text{Co}_2$ magnet, the present calculations indicate that it could be fabricated in bulk based on its thermodynamic stability and exhibits values for $\mu_0 M_s = 1.31$ – 1.39 T (depending on the model); and has an excellent value for $\mu_0 H_a$ equal to 11.568 T; a high T_c value of 731.89 K; and $\kappa = 2.101 > 1$.

Table 9 summarizes the intrinsic properties of some reported [3,12–15,32] ThMn₁₂-type structure magnets that are compared to the characteristics for Neomax [4,16,43] along with our present results of calculations for the $(\text{Sm}_{0.8}\text{Zr}_{0.2})\text{Ni}_4(\text{Fe}_{0.8}\text{Co}_{0.2})_8$ and $(\text{Ce}_{0.5}\text{Sm}_{0.5})\text{Ni}_4\text{Fe}_6\text{Co}_2$ magnets. The maximum energy product of the $(\text{Sm}_{0.8}\text{Zr}_{0.2})\text{Ni}_4(\text{Fe}_{0.8}\text{Co}_{0.2})_8$ and $(\text{Ce}_{0.5}\text{Sm}_{0.5})\text{Ni}_4\text{Fe}_6\text{Co}_2$ magnets is $\sim 79\%$ and 66% of the maximum energy product of Neomax, respectively; the anisotropy field of the $(\text{Ce}_{0.5}\text{Sm}_{0.5})\text{Ni}_4\text{Fe}_6\text{Co}_2$ magnet is the largest among the listed magnets with ThMn₁₂-type structure, and the Curie temperature exceeds that of Neomax by 340 K and 143 K for the $(\text{Sm}_{0.8}\text{Zr}_{0.2})\text{Ni}_4(\text{Fe}_{0.8}\text{Co}_{0.2})_8$ and $(\text{Ce}_{0.5}\text{Sm}_{0.5})\text{Ni}_4\text{Fe}_6\text{Co}_2$ magnets, respectively. Comparing the maximum energy products of our earlier suggested magnets with ThMn₁₂-type structure [34–38], the novel $(\text{Sm}_{0.8}\text{Zr}_{0.2})\text{Ni}_4(\text{Fe}_{0.8}\text{Co}_{0.2})_8$ magnet ($|BH|_{\max} = 406$ kJ/m³) outperforms the $\text{SmNi}_4(\text{Fe}_{0.9}\text{Co}_{0.1})_8$, SmCoNiFe_3 , and $\text{YFe}_3(\text{Ni}_{0.3}\text{Co}_{0.7})_2$ magnets with $|BH|_{\max} = 382$ kJ/m³, 361 kJ/m³, and 351 kJ/m³, respectively.

Table 9. Saturation magnetization, anisotropy field, Curie temperature, and maximum energy product values of 1:12 magnets and Nd₂Fe₁₄B₁.

Material	$\mu_0 M_s$ (T)	$\mu_0 H_a$ (T)	T_c (K)	$ BH _{\max}$ ($\frac{\text{kJ}}{\text{m}^3}$)	References
Nd ₂ Fe ₁₄ B ₁	1.61	7.6	588	515	[4,16,43]
$(\text{Sm}_{0.8}\text{Zr}_{0.2})(\text{Fe}_{0.75}\text{Co}_{0.25})_{11.5}\text{Ti}_{0.5}$	1.58	7.41	880	495	[13]
$(\text{Sm}_{0.8}\text{Y}_{0.2})(\text{Fe}_{0.80}\text{Co}_{0.20})_{11.5}\text{Ti}_{0.5}$	1.50	11.0	820	447	[14,15]
$\text{Sm}_{0.94}(\text{Fe}_{0.81}\text{Co}_{0.19})_{11}\text{Ti}_{1.08}$	1.43	10.9	800	406	[12]
$(\text{Sm}_{0.77}\text{Zr}_{0.24})(\text{Fe}_{0.80}\text{Co}_{0.19})_{11.5}\text{Ti}_{0.65}$	1.53	8.4	830	465	[12]
$(\text{Sm}_{0.92}\text{Zr}_{0.08})(\text{Fe}_{0.75}\text{Co}_{0.25})_{11.35}\text{Ti}_{0.65}$	1.47	>9.0	843	429	[3]
$(\text{Ce}_{0.5}\text{Sm}_{0.5})\text{Ti}_1\text{Co}_2\text{Fe}_9$	1.15	5.60	726	261	[32]
$(\text{Sm}_{0.75}\text{Zr}_{0.25})\text{Ni}_4(\text{Fe}_{0.8}\text{Co}_{0.2})_8$	1.43	4.28	828	406	Present
$(\text{Ce}_{0.5}\text{Sm}_{0.5})\text{Ni}_4\text{Fe}_6\text{Co}_2$	1.31	11.57	731	342	Present

According to our calculations, the maximum energy product of the $(\text{Sm}_{0.8}\text{Zr}_{0.2})\text{Ni}_4\text{Fe}_8$ magnet, $|BH|_{\max} = 407.21$ kJ/m³, (see Table 3) is larger than the undoped SmNi_4Fe_8 magnet, which has a $|BH|_{\max} = 377.6$ kJ/m³ [38]. As was discovered by Tozman et al. [17], the addition of Zr to the SmFe_{12} magnet not only stabilized it in the ThMn₁₂-type structure, but in addition, it increased the saturation magnetization of the $\text{Sm}(\text{Fe}_{0.8}\text{Co}_{0.2})_{12}$ magnet in the thin film form. A similar phenomenon occurs in the case of the SmNi_4Fe_8 compound. It is well known that the spins of the samarium and TM (iron, cobalt, and nickel) atoms adjust in an antiparallel direction; however, the total spin moment of the SmFe_{12} compound aligns parallel to the spin moments of TM. Zr substitution for Sm decreases the magnetic moment on the 2a site and, thus, increases the total magnetic moment of the $(\text{Sm}_{1-x}\text{Zr}_x)\text{Fe}_{12}$ magnets. The reasons are straightforward, since the 4f electrons on samarium spin polarize and thus produce a spin moment. Replacing a fraction of Sm with Zr, that has no occupied 4f levels thus reduces the amount of 4f electrons and the spin moment. A charge transfer of d electrons from Zr to Fe increases the spin moment on iron. Therefore, if one

can replace Sm with Zr, it reduces or eliminates the need for the expensive rare-earth metal and also improves the total magnetic moment of the compound. The same arguments are true for the $(\text{Sm}_{1-x}\text{Zr}_x)\text{Ni}_4\text{Fe}_8$ magnets studied in the present work.

Recently, Kobayashi et al. [45] performed X-ray absorption fine structure (XAFS) and scanning transmission electron microscopy (STEM) to understand the magnetization increase associated with Zr replacement in the $(\text{Sm}_{1-x}\text{Zr}_x)(\text{Fe}_{0.8}\text{Co}_{0.2})_{12}$ alloys. They confirmed that the magnetic moment of Sm was two orders of magnitude smaller than the magnetic moment of Fe and Co, and thus the contribution to the total magnetization from 2a sites, occupied by Sm and Zr, is negligible. In addition, they found that the charge transfer from Zr (2a sites) atoms to the Fe (8f sites) atoms drives a magnetization increase in the $(\text{Sm}_{1-x}\text{Zr}_x)(\text{Fe}_{0.8}\text{Co}_{0.2})_{12}$ single crystalline films. By performing ab initio calculations, Matsumoto et al. [46] found that Zr(2a)-induced an increase in magnetization due to rearrangement (charge transfer) of the 4d-electron states from Zr to Fe sites, reducing the overlap of the majority-spin states on the Fermi level for Fe (8f). This is identical to the Slater-Pauling curve in the $\text{Fe}_{1-x}\text{Co}_x$ alloys, where cobalt sums up one electron on the top of the 3d-electron band of iron; in the case of the $(\text{Sm,Zr})\text{Fe}_{12}$ compound, the delocalized 4d-electrons of zirconium sum up one electron on the top of the 3d-electron band of iron.

In the case when Ce substitutes for Sm, the calculated maximum energy product also increases from $|BH|_{\max} = 377.6 \text{ kJ/m}^3$ for the SmNi_4Fe_8 magnet [38] to 386.0 kJ/m^3 for the $(\text{Ce}_{0.5}\text{Sm}_{0.5})\text{Ni}_4\text{Fe}_6\text{Co}_2$ magnet. In this case, the increase in saturation magnetization is due to the decrease in the magnetic moment of the 2a sites that are equally occupied by Ce and Sm atoms. Analogous to the discussion above, cerium substitution for samarium decreases the number of spin-polarized 4f electrons because cerium has only about 1 4f electron while samarium has about five. The result is a smaller spin moment on the (2a) site and a larger total magnetic moment for the compound.

Numerous theoretical studies have been performed to understand the stability of the REFe_{12} compound, which decomposes into the $\text{RE}_2\text{Fe}_{17}$ compound and $\alpha\text{-Fe}$ [27,46–53]. According to Fukazawa et al. [53], the stability of $(\text{RE}_{1-y}\text{Zr}_y)(\text{Fe}_{1-x}\text{Co}_x)_{12}$ alloys exhibits general tendencies that are similar for $\text{RE}=\text{Y, Nd, and Sm}$: the stability of the 1:12 phase relative to the 2:17 ($\text{Th}_2\text{Zn}_{17}$ -type structure) phase increases as Zr concentration increases and Co concentration decreases.

As was shown in Ref. [38], the $\text{SmNi}_4(\text{Fe}_{1-x}\text{Co}_x)_8$ alloys have a negative formation energy relative to the unary systems $\alpha\text{-Sm}$, $\alpha\text{-Fe}$, $\alpha\text{-Co}$, and $\alpha\text{-Ni}$, the whole composition range, with a pronounced minimum of -2.85 mRy/atom at $x \approx 0.4$. According to the present calculations (Figure 2), the heat of formation of the $(\text{Sm}_{0.8}\text{Zr}_{0.2})\text{Ni}_4(\text{Fe}_{1-x}\text{Co}_x)_8$ alloys, relative to the unary systems $\alpha\text{-Sm}$, $\alpha\text{-Zr}$, $\alpha\text{-Fe}$, $\alpha\text{-Co}$, and $\alpha\text{-Ni}$, is also negative, reaching a minimum value of -3.26 mRy/atom at $x \approx 0.45$. Both Ni and Zr play the role of stabilizers for the $(\text{Sm}_{0.8}\text{Zr}_{0.2})\text{Ni}_4(\text{Fe}_{1-x}\text{Co}_x)_8$ alloys, and a decrease in the maximum value of the formation energy from -2.85 mRy/atom ($\text{SmNi}_4(\text{Fe}_{0.6}\text{Co}_{0.4})_8$) to -3.26 mRy/atom ($(\text{Sm}_{0.8}\text{Zr}_{0.2})\text{Ni}_4(\text{Fe}_{0.55}\text{Co}_{0.45})_8$) implies the $(\text{Sm}_{0.8}\text{Zr}_{0.2})\text{Ni}_4(\text{Fe}_{1-x}\text{Co}_x)_8$ alloys will be stable against decomposition to the $\text{Th}_2\text{Zn}_{17}$ -type structure compound and the respective TMs.

The $(\text{Ce}_{0.5}\text{Sm}_{0.5})\text{Ni}_4\text{Co}_2\text{Fe}_6$ alloy is fairly stable with respect to the elements $\alpha\text{-Sm}$, $\alpha\text{-Ce}$, $\alpha\text{-Fe}$, $\alpha\text{-Co}$, and $\alpha\text{-Ni}$ and exhibits a significantly negative calculated formation energy of -5.735 mRy/atom . The $(\text{Ce}_{0.5}\text{Sm}_{0.5})\text{Ni}_4\text{Co}_2\text{Fe}_6$ magnet is also predicted to be stable against decomposition into the $\text{Th}_2\text{Zn}_{17}$ -type structure compound and its respective TMs.

In conclusion, we showed that the $(\text{Sm}_{0.8}\text{Zr}_{0.2})(\text{Fe}_{1-x}\text{Co}_x)_{12}$ alloys could be stabilized by substituting a significant quantity of Fe or Co atoms with Ni atoms. These modern permanent magnets are predicted to have excellent magnetic characteristics, specifically a significant gain energy product ($(\text{Sm}_{0.8}\text{Zr}_{0.2})\text{Ni}_4(\text{Fe}_{0.9}\text{Co}_{0.1})_8$) and anisotropy field ($(\text{Sm}_{0.5}\text{Ce}_{0.5})\text{Ni}_4\text{Fe}_6\text{Co}_2$), as well as a high Curie temperature that substantially surpasses Neomax magnets. However, it is imperative to mention that, though these intrinsic properties are necessary for permanent magnets, this alone is not a sufficient requirement. It is also necessary for the anisotropic microstructure of a magnet to exhibit both significant values for coercivity and remanence [6–8,25,34,45,53–65]. It is therefore necessary to

establish a pertinent grain boundary phase that can grow in equilibrium with the matrix phase in order to improve the extrinsic magnetic properties.

Author Contributions: Conceptualization, A.L.; methodology, A.L. and P.S.; writing-review and editing, A.L., P.S., A.P., and E.E.M. All authors have read and agreed to the published version of the manuscript.

Funding: This research is supported by the Critical Materials Innovation Hub, an Energy Innovation Hub funded by the US Department of Energy, Office of Energy Efficiency and Renewable Energy, Advanced Materials and Manufacturing Technologies Office.

Data Availability Statement: The data presented in this study are available in the present article.

Acknowledgments: The work was performed under the auspices of the US Department of Energy by the Lawrence Livermore National Laboratory under Contract No. DE-AC52-07NA27344. A. L. thanks A. Ruban, O. Peil, P. Korzhavyi, and L. Vitos for their technical support.

Conflicts of Interest: The authors declare no conflicts of interest.

References

- Hirayama, Y.; Takahashi, Y.; Hirosawa, S.; Hono, K. Intrinsic hard magnetic properties of $\text{Sm}(\text{Fe}_{1-x}\text{Co}_x)_{12}$ compound with the ThMn_{12} structure. *Scr. Mater.* **2017**, *138*, 62–65.
- Buschow, K.H.J. Permanent magnet materials based on tetragonal rare earth compounds of the type $\text{RFe}_{12-x}\text{M}_x$. *J. Magn. Magn. Mater.* **1991**, *100*, 79–89.
- Gabay, A.M.; Hadjipanayis, G.C. Recent developments in RFe_{12} -type compounds for permanent magnets. *Scr. Mater.* **2018**, *154*, 284–288.
- Coey, J.M.D. Perspective and prospects for rare earth permanent magnets. *Eng. J.* **2020**, *6*, 119–131.
- Hadjipanayis, G.C.; Gabay, A.M.; Schonhobel, A.M.; Martin-Cid, A.; Barandiaran, J.M.; Niarchos, D. ThMn_{12} -Type Alloys for permanent magnets. *Eng. J.* **2020**, *6*, 141–147.
- Takahashi, Y.K.; Sepehri-Amin, H.; Ohkubo, T. Recent advances in SmFe_{12} -based permanent magnates. *STAM* **2021**, *22*, 449–460.
- Tozman, P.; Sepehri-Amin, H.; Hono, K. Prospects for the development of SmFe_{12} -based permanent magnets with a ThMn_{12} -type phase. *Scr. Mater.* **2021**, *194*, 113686.
- Tozman, P.; Sepehri-Amin, H.; Tang, X.; Ohkubo, T.; Hono, K. Development of Co-lean $(\text{Sm},\text{Y})(\text{Fe},\text{Co},\text{Ti})_{12}$ compounds with large saturation magnetization. *Appl. Phys. Expr.* **2022**, *15*, 045505.
- Coehoorn, R. Electronic structure and magnetism of transition-metal-stabilized $\text{YFe}_{12-x}\text{M}_x$ intermetallic compounds. *Phys. Rev. B* **1990**, *41*, 11790–11797.
- Ohashi, K.; Tawara, Y.; Osugi, R.; Shimao, M. Magnetic properties of Fe-rich rare-earth intermetallic compounds with a ThMn_{12} structure. *J. Appl. Phys.* **1988**, *64*, 5714–5716.
- Hu, B.P.; Li, H.S.; Gavigan, J.P.; Coey, J.M.D. Intrinsic magnetic properties of the iron-rich ThMn_{12} -structure alloys $\text{R}(\text{Fe}_{11}\text{Ti})$; $\text{R} = \text{Y}, \text{Nd}, \text{Sm}, \text{Gd}, \text{Tb}, \text{Dy}, \text{Ho}, \text{Er}, \text{Tm}$ and Lu . *J. Phys. Condens. Matter* **1989**, *1*, 755–770.
- Tozman, P.; Sepehri-Amin, H.; Takahashi, Y.K.; Hirosawa, S.; Hono, K. Intrinsic magnetic properties of $\text{Sm}(\text{Fe}_{1-x}\text{Co}_x)_{11}\text{Ti}$ and Zr-substituted $\text{Sm}_{1-y}\text{Zr}_y\text{Fe}_{0.8}\text{Co}_{0.2}(\text{Ti}_{0.5})_{11.5}\text{Ti}_{0.5}$ compounds with ThMn_{12} structure toward the development of permanent magnets. *Acta Mater.* **2018**, *153*, 354–363.
- Kuno, T.; Suzuki, S.; Urushibata, K.; Kobayashi, K.; Sakuma, N.; Yano, M.; Kato, A.; Manabe, A. $(\text{Sm},\text{Zr})(\text{Fe},\text{Co})_{11.0-11.5}\text{Ti}_{1.0-0.5}$ compounds as new permanent magnet materials. *AIP Adv.* **2016**, *6*, 025221.
- Hagiwara, M.; Sanada, N.; Sakurada, S. Effect of Y substitution on the structural and magnetic properties of $\text{Sm}(\text{Fe}_{0.8}\text{Co}_{0.2})_{11.4}\text{Ti}_{0.6}$. *J. Magn. Magn. Mater.* **2018**, *465*, 554–558.
- Hagiwara, M.; Sanada, N.; Sakurada, S. Structure and magnetic properties of rapidly quenched $(\text{Sm},\text{R})(\text{Fe},\text{Co})_{11.4}\text{Ti}_{0.6}$. *AIP Adv.* **2019**, *9*, 035036.
- Matsuura, Y. Recent development of Nd-Fe-B sintered magnets and their applications. *J. Magn. Magn. Mater.* **2006**, *303*, 344–347.
- Tozman, P.; Takahashi, Y.K.; Sepehri-Amin, H.; Ogawa, D.; Hirosawa, S.; Hono, K. The effect of Zr substitution on saturation magnetization in $(\text{Sm}_{1-x}\text{Zr}_x)(\text{Fe}_{0.8}\text{Co}_{0.2})_{12}$ compound with the ThMn_{12} structure. *Acta Mater.* **2019**, *178*, 114–121.
- Tozman, P.; Sepehri-Amin, H.; Zhang, L.T.; Wang, J.; Xu, X.D.; Hono, K. An alternative approach to the measurement of anisotropy field—Single grain extraction. *J. Magn. Magn. Mater.* **2020**, *494*, 165747.
- Kim, H.T.; Kim, Y.B.; Kim, C.S.; Kim, T.K.; Jin, H. Magnetocrystalline anisotropy of $(\text{Sm}_{0.5}\text{RE}_{0.5})\text{Fe}_{11}\text{Ti}$ compounds ($\text{RE} = \text{Ce}, \text{Pr}, \text{Nd}, \text{Sm}, \text{Gd}$ and Tb). *J. Magn. Magn. Mater.* **1996**, *152*, 387–390.
- Zhou, C.; Tessema, M.; Meyer, M.S.; Pinkerton, F.E. Synthesis of $\text{CeFe}_{10.5}\text{Mo}_{1.5}$ with ThMn_{12} -type structure by melt spinning. *J. Magn. Magn. Mater.* **2013**, *336*, 26–28.
- Zhou, C.; Pinkerton, F.E.; Herbst, J.F. Magnetic properties of $\text{CeFe}_{11-x}\text{Co}_x\text{Ti}$ with ThMn_{12} structure. *J. Appl. Phys.* **2014**, *115*, 17C716.

22. Zhou, C.; Sun, K.; Pinkerton, F.E.; Kramer, M.J. Magnetic hardening of $Ce_{1-x}Fe_{1-y}Co_yTi$ with $ThMn_{12}$ structure by melt spinning. *J. Appl. Phys.* **2015**, *117*, 17A741.
23. Ke, L.; Johnson, D.D. Intrinsic magnetic properties in $R(Fe_{1-x}Co_x)_{11}TiZ$ ($R = Y$ and Ce ; $Z = H, C,$ and N). *Phys. Rev. B* **2016**, *94*, 244231.
24. Martinez-Casado, R.; Dasmahapatra, A.; Sgroi, M.F.; Romero-Muñiz, C.; Herper, H.C.; Vekilova, O.Y.; Ferrari, A.M.; Pullini, D.; Desmarais, J.; Maschio, L. The $CeFe_{11}Ti$ permanent magnet: A closer look at the microstructure of the compound. *J. Phys. Condens. Matter* **2019**, *31*, 505505.
25. Harashima, Y.; Fukazawa, T.; Miyake, T. Cerium as a possible stabilizer of $ThMn_{12}$ -type iron-based compounds: A first-principles study. *Scr. Mater.* **2020**, *179*, 12–15.
26. Dasmahapatra, A.; Martinez-Casado, R.; Romero-Muñiz, C.; Sgroi, M.F.; Ferrari, A.M.; Maschio, L. Doping the permanent magnet $CeFe_{11}Ti$ with Co and Ni using ab-initio density functional methods. *Phys. B* **2021**, *620*, 413241.
27. Bhandari, C.; Paudyal, D. Enhancing stability and magnetism of $ThMn_{12}$ -type cerium-iron intermetallics by site substitution. *Phys. Rev. Res.* **2022**, *4*, 023012.
28. Goll, D.; Loeffler, R.; Stein, R.; Pflanz, U.; Goeb, S.; Karimi, R.; Schneider, G. Temperature dependent magnetic properties and application potential of intermetallic $Fe_{11-x}Co_xTiCe$. *Phys. Status Solidi* **2014**, *8*, 862–865.
29. Gabay, A.M.; Martín-Cid, A.; Salazar, D.; Barandiaran, J.M.D.; Hadjipanayis, G.C. Low-cost $Ce_{1-x}Sm_x(Fe, Co, Ni)_{12}$ alloys for permanent magnets. *AIP Adv.* **2016**, *6*, 056015.
30. Martín-Cid, A.; Gabay, A.M.; Salazar, D.; Barandiaran, J.M.; Hadjipanayis, G.C. Tetragonal Ce-based Ce-Sm(Fe, Co, Ni)₁₂ alloys for permanent magnets. *Phys. Status Solidi C* **2016**, *13*, 962–964.
31. Wuest, H.; Bommer, L.; Huber, A.M.; Goll, D.; Weissgaerber, T.; Kieback, B. Preparation of nanocrystalline $Ce_{1-x}Sm_x(Fe,Co)_{11}Ti$ by melt spinning and mechanical alloying. *J. Magn. Magn. Mater.* **2017**, *428*, 194–197.
32. Martín-Cid, A.; Salazar, D.; Schönhöbel, A.M.; Garitaonandia, J.S.; Barandiaran, J.M.; Hadjipanayis, G.C. Magnetic properties and phase stability of tetragonal $Ce_{1-x}Sm_xFe_9Co_2Ti$ 1:12 phase for permanent magnets. *J. Alloys Compd.* **2018**, *749*, 640–644.
33. Martín-Cid, A. Development of New High Anisotropy Phases for Permanent Magnet Applications. Ph.D. Thesis, University of the Basque Country, Leioa, Spain, 2018; pp. 67–101.
34. Saito, T. Magnetic Properties of (Ce, Sm)Fe₁₁Ti Magnets, *Mater. Trans.* **2022**, *63*, 1097–1100.
35. Söderlind, P.; Landa, A.; Loch, I.L.M.; Åberg, D.; Kvashnin, Y.; Pereiro, M.; Däne, M.; Turchi, P.E.A.; Antropov, V.P.; Eriksson, O. Prediction of the new efficient permanent magnet $SmCoNiFe_3$. *Phys. Rev. B* **2017**, *96*, 100404.
36. Landa, A.; Söderlind, P.; Parker, D.; Åberg, D.; Lordi, V.; Perron, A.; Turchi, P.E.A.; Chouhan, R.K.; Paudyal, D.; Lograsso, T.A. Thermodynamics of the $SmCo_5$ compound doped with Fe and Ni: An ab initio study. *J. Alloys Compd.* **2018**, *765*, 659–663.
37. Landa, A.; Söderlind, P.; Moore, E.E.; Perron, A. Thermodynamics and magnetism of YCo_5 compound doped with Fe and Ni: An ab initio study. *Appl. Sci.* **2020**, *10*, 6037.
38. Landa, A.; Söderlind, P.; Moore, E.E.; Perron, A. Thermodynamics and Magnetism of $SmFe_{12}$ Compound Doped with Co and Ni: An Ab Initio Study. *Appl. Sci.* **2022**, *12*, 4860.
39. Momma, K.; Izumi, F. VESTA 3 for three-dimensional visualization of crystal, volumetric and morphology data. *J. Appl. Crystallogr.* **2011**, *44*, 1272–1276.
40. Odkhuu, D.; Ochirkhuyag, T.; Hong, S.C. Enhancing energy product and thermal stability of $SmFe_{12}$ by interstitial doping. *Phys. Rev. Appl.* **2020**, *13*, 54076.
41. Sato, K.; Katayama-Yoshida, H.; Dederichs, P. Dilute magnetic semiconductors. *Newsletter* **2005**, *70*, 93–110.
42. Ma, D.; Grabowski, B.; Körmann, F.; Neugebauer, J.; Raabe, D. Ab initio thermodynamics of the $CoCrFeMnNi$ high entropy alloy: Importance of entropy contributions beyond the configurational one. *Acta Mater.* **2015**, *100*, 90–97.
43. Coey, J.M.D. Hard magnetic materials: A Perspective. *IEEE Trans. Magn.* **2011**, *47*, 4671–4681.
44. Skomski, R.; Coey, J.M.D. Magnetic anisotropy—How much is enough for a permanent magnet? *Scr. Mater.* **2016**, *112*, 3–8.
45. Kobayashi, S.; Ogawa, D.; Xu, X.D.; Takahashi, Y.K.; Martín-Cid, A.; Ishigami, K.; Kotani, Y.; Suzuki, M.; Yoshioka, T.; Tsuchiura, H.; et al. Multimodal analysis of Zr substitution effects on magnetic and crystallographic properties in $(Sm_{1-x}Zr_x)(Fe_{0.8}Co_{0.2})_{12}$ compounds with $ThMn_{12}$ structure. *Acta Mater.* **2023**, *242*, 118454.
46. Matsumoto, M.; Hawaii, T.; Ono, K. (Sm, Zr)Fe_{12-x}M_x (M = Zr, Ti, Co) for permanent-magnet applications: Ab initio material design integrated with experimental characterization. *Phys. Rev. Appl.* **2020**, *13*, 64028.
47. Harashima, Y.; Terakura, K.; Kino, H.; Ishibashi, S.; Miyake, T. First-principles study on stability and magnetism of $NdFe_{11}M$ and $NdFe_{11}MN$ for $M = Ti, V, Cr, Mn, Fe, Co, Ni, Cu, Zn$. *J. Appl. Phys.* **2016**, *120*, 203904.
48. Harashima, Y.; Fukazawa, T.; Kino, H.; Miyake, T. Effect of R-site substitution and pressure on stability of RFe_{12} a first-principles study. *J. Appl. Phys.* **2018**, *124*, 163902.
49. Fukazawa, T.; Harashima, Y.; Hou, Z.; Miyake, T. Bayesian optimization of chemical composition: A comprehensive framework and its application to RFe_{12} -type magnet compounds. *Phys. Rev. Mater.* **2019**, *3*, 53807.
50. Schönhöbel, A.M.; Madugundo, R.; Vekilova, O.Y.; Eriksson, O.; Herper, H.C.; Barandiarán, J.M.; Hadjipanayis, G.C. Intrinsic magnetic properties of $SmFe_{12-x}V_x$ alloys with reduced V-concentration. *J. Alloys Compd.* **2019**, *786*, 969–974.
51. Dirba, I.; Harashima, Y.; Sepehri-Amin, H.; Ohkubo, T.; Miyake, T.; Hirotsawa, S.; Hono, K. Thermal decomposition of $ThMn_{12}$ -type phase and its optimum stabilizing elements in $SmFe_{12}$ -based alloys. *J. Alloys Compd.* **2020**, *813*, 152224.
52. Fukazawa, T.; Harashima, Y.; Miyake, T. First-principles study on the stability of $(R, Zr)(Fe, Co, Ti)_{12}$ against 2-17 and unary phases ($R = Y, Nd, Sm$). *Phys. Rev. Mater.* **2022**, *6*, 054404.

53. Makurenkova, A.; Ogawa, D.; Tozman, P.; Okamoto, S.; Nikitin, S.; Hirosawa, S.; Hono, K.; Takahashi, Y.K. Intrinsic hard magnetic properties of $\text{Sm}(\text{Fe},\text{Co})_{12-x}\text{Ti}_x$ compound with ThMn_{12} structure. *J. Alloys Compd.* **2021**, *861*, 158477.
54. Maccari, F.; Ener, S.; Koch, D.; Dirba, I.; Skokov, K.P.; Bruder, E.; Schäfer, L.; Gutfleisch, O. Correlating changes of the unit cell parameters and microstructure with magnetic properties in the $\text{CeFe}_{11}\text{Ti}$ compound. *J. Alloys Compd.* **2021**, *867*, 158805.
55. Srinithi, A.K.; Sepehri-Amina, H.; Tang, X.; Tozman, P.; Li, J.; Zhang, J.; Kobayashi, S.; Ohkubo, T.; Nakamura, T.; Hono, K. Phase relations and extrinsic magnetic properties of $\text{Sm}-(\text{Fe},\text{Co})-\text{Ti}-(\text{Ga})$ -based alloys for ThMn_{12} -type permanent magnets. *J. Magn. Magn. Mater.* **2021**, *529*, 167866.
56. Gabay, A.M.; Hadjipanayis, G.C. High-coercivity ThMn_{12} -type monocrystalline $\text{Sm}-\text{Zr}-\text{Fe}-\text{Co}-\text{Ti}$ particles by high-temperature reduction diffusion. *Scr. Mater.* **2021**, *196*, 113760.
57. Niarchos, D.; Gjoka, M.; Schönhöbel, A.M.; Aubert, A.; Madugundo, R.; Garitaonandí, J.J.S.J.; Barandiaranb, J.M.; Hadjipanayi, G. Intrinsic magnetic properties of $(\text{Nd}_{1-x}\text{Sm}_x)\text{Fe}_{11}\text{Ti}$. *J. Alloys Compd.* **2021**, *864*, 158097.
58. Tozman, P.; Sepehri-Amin, H.; Ohkubo, T.; Hono, K. Intrinsic magnetic properties of $(\text{Sm},\text{Gd})\text{Fe}_{12}$ -based compounds with minimized addition of Ti. *J. Alloys Compd.* **2021**, *855*, 157491.
59. Gabay, A.M.; Han, C.; Ni, C.; Hadjipanayis, G.C. Effect of alloying with Sc, Nb and Zr on reduction-diffusion synthesis of magnetically hard $\text{Sm}(\text{Fe},\text{Co},\text{Ti})_{12}$ -based monocrystalline powders. *J. Magn. Magn. Mater.* **2022**, *541*, 168550.
60. Ochirkhuyag, T.; Hong, S.C.; Odkhuu, D. Intrinsic hard magnetism and thermal stability of a ThMn_{12} -type permanent magnet. *npj Comput. Mater.* **2022**, *8*, 193.
61. Tozman, P.; Fukazawa, T.; Ogawa, D.; Sepehri-Amin, H.; Bolyachkin, A.; Miyake, T.; Hirosawa, S.; Hono, K.; Takahashi, Y.K. Peculiar behavior of V on the Curie temperature and anisotropy field of $\text{SmFe}_{12-x}\text{V}_x$ compounds. *Acta Mater.* **2022**, *232*, 117928.
62. Gabay, A.M.; Hadjipanayis, G.C. Microstructure and hard magnetic properties of $\text{Sm}_{1-x}\text{Zr}_x(\text{Fe},\text{Co})_{11.3-y}\text{Ti}_{0.7}$ by ingots and thick melt-spun ribbons. *IEEE Trans. Magn.* **2022**, *58*, 2100805.
63. Ogawa, D.; Fukazawa, T.; Li, S.; Ueno, T.; Sakai, S.; Mitsui, T.; Miyake, T.; Okamoto, S.; Hirosawa, S.; Takahashi, Y.K. Temperature dependence of site-resolved Fe magnetic moments in ThMn_{12} -type $\text{Sm}(\text{Fe}_{1-x}\text{Co}_x)_{12}$ compounds studied via synchrotron Mössbauer spectroscopy. *J. Magn. Magn. Mater.* **2022**, *552*, 169188.
64. Srinithi, A.K.; Tang, X.; Sepehri-Amina, H.; Zhang, J.; Ohkubo, T.; Hono, K. High-coercivity SmFe_{12} -based anisotropic sintered magnets by Cu addition. *Acta Mater.* **2023**, *256*, 119911.
65. Han, C.; Gabay, A.M.; Ni, C.; Hadjipanayis, G.C. Structural characteristics and phase evolution of calcium-reduced $(\text{Sm},\text{Zr})(\text{Fe},\text{Co},\text{Ti})_{12}$ particles. *Microsc. Microanal.* **2023**, *29* (Suppl. S1), 1328–1329.

Disclaimer/Publisher's Note: The statements, opinions and data contained in all publications are solely those of the individual author(s) and contributor(s) and not of MDPI and/or the editor(s). MDPI and/or the editor(s) disclaim responsibility for any injury to people or property resulting from any ideas, methods, instructions or products referred to in the content.